Impact of scour on lateral resistance of wind turbine monopiles

An experimental study

Li, Q.; Askarinejad, A.; Gavin, K.

DOI
10.1139/cgj-2020-0219

Publication date
2021

Document Version
Final published version

Published in
Canadian Geotechnical Journal

Citation (APA)
Li, Q., Askarinejad, A., & Gavin, K. (2021). Impact of scour on lateral resistance of wind turbine monopiles: An experimental study. *Canadian Geotechnical Journal*, *58*(11), 1770-1782. https://doi.org/10.1139/cgj-2020-0219

Canadian Science Publishing

ARTICLE

Impact of scour on lateral resistance of wind turbine monopiles: an experimental study

Q. Li, A. Askarinejad, and K. Gavin

Abstract: The majority of offshore wind structures are supported on large-diameter, rigid monopile foundations. These piles may be subjected to scour due to the waves and currents that causes a loss of soil support and consequently decreases the pile capacity and system stiffness. The results of numerical models suggest that the shape of the scour hole affects the magnitude of pile capacity loss; however, there is a dearth of experimental test data that quantify this effect. This paper presents a series of centrifuge model tests on an instrumented model pile that investigates the effects of scour-hole geometry on the response of a laterally loaded pile embedded in sand. The pile instrumentation allowed load–displacement and *p*–*y* (soil reaction – displacement) curves to be derived. Three scour geometries (global, local wide, and local narrow) and three scour depths (1*D*, 1.5*D*, and 2*D*; where *D* is pile diameter) were modelled. For all three scour types, pile moment capacity decreased almost linearly with increase of scour depth. Simple empirical relations were proposed to evaluate the detrimental influence of scour on the pile moment capacity. A new method has been developed to allow designers to quantify the effect of scour-hole shape and severity of scour on the pile response.

Key words: offshore wind monopiles, scour, moment capacity, centrifuge modelling, scour-hole shapes, *p*–*y* curves.

Résumé : La majorité des structures éoliennes offshore reposent sur des fondations monopiles rigides de grand diamètre. Ces pieux peuvent être soumis à l'affouillement dû aux vagues et aux courants, ce qui entraîne une perte de support du sol et, par conséquent, une diminution de la capacité des pieux et de la rigidité du système. Les résultats des modèles numériques suggèrent que la forme du trou d'affouillement affecte l'ampleur de la perte de capacité des piles, Cependant, les données expérimentales permettant de quantifier cet effet sont rares. Cet article présente une série de tests de modèles de centrifugeuses sur une pile modèle instrumentée qui étudie les effets de la géométrie des trous d'affouillement sur la réponse d'une pile chargée latéralement et enfoncée dans le sable. L'instrumentation des pieux a permis de dériver les courbes de charge–déplacement et *p*–*y* (réaction – déplacement du sol). Trois géométries d'affouillement (globale, locale large et locale étroite) et trois profondeurs d'affouillement (1*D*, 1,5*D* et 2*D*; où *D* est le diamètre des pieux) ont été modélisées. Pour les trois types d'affouillement, la capacité de moment de pieu a diminué presque linéairement avec l'augmentation de la profondeur d'affouillement. Des relations empiriques simples ont été proposées pour évaluer l'influence néfaste de l'affouillement sur la capacité de moment de pieu. Une nouvelle méthode a été mise au point pour permettre aux concepteurs de quantifier l'effet de la forme du trou d'affouillement et de la gravité de l'affouillement sur la réponse du pieu. [Traduit par la Rédaction]

Mots-clés : monopiles de vent en mer, scour, capacité de moment, modélisation de centrifugeuse, formes de trous de scour, courbes *p*–*y*.

1. Introduction

Monopiles are the most economical foundation system for offshore wind turbines (OWTs) installed in shallow coastal waters (Byrne et al. 2019). The typical slenderness ratio (*L*/*D*; where *L* is embedded length and *D* is diameter) for OWT monopiles is between 3 and 6 (Doherty and Gavin 2012; Wu et al. 2019). Cylindrical structures such as OWT monopiles are prone to loss of soil support due to sand erosion, i.e., scour. Consequently, the pile lateral capacity and stiffness could be decreased, potentially resulting in large lateral displacement and rotation. Such effects can put the superstructure at risk through the generation of excessive fatigue loading as well as operational issues (Li et al. 2018). The shapes of various types of scour holes are illustrated in Fig. 1. Typically, scour holes are formed in a shape approximating an inverted frustum. The slope angle (ω) is roughly equal to the angle of repose of sand, generally in the range of 30° to 44° (Richardson and Davis 2001), and the top scour width (W_t) is often assumed to be twice the scour depth (Richardson and Davis 2001; Lin et al. 2014). Based on several experimental studies, it has been shown that the scour depth (D_s) depends on the diameter of the pile (D), Froude number of the water flow, shear stress applied to the sand surface due to the flow, and soil strength (Jones et al. 1992; Sørensen and Ibsen 2013). Det Norske Veritas (DNV 2014) suggested the adoption of an extreme scour depth of 2*D*. However, Sørensen and Ibsen (2013) illustrated that this assumption ($D_s = 2D$) might be too conservative for wave-induced scour holes.

One approach, and perhaps the simplest, to model the effect of scour on the lateral behaviour of a monopile is to remove the affected soil layer completely. This approach simulates a so-called global scour condition (schematized on the left-hand side of Fig. 1). Based on various numerical analyses, Li et al. (2013), Lin

Received 8 April 2020. Accepted 2 December 2020.

Q. Li, A. Askarinejad, and K. Gavin. Faculty of Civil Engineering and Geosciences, Delft University of Technology, Stevinweg 1, 2628 CN Delft, the Netherlands.

Corresponding author: A. Askarinejad (email: A.Askarinejad@tudelft.nl).

Fig. 1. Symbols and definitions of scour hole (modified after Li et al. 2020).

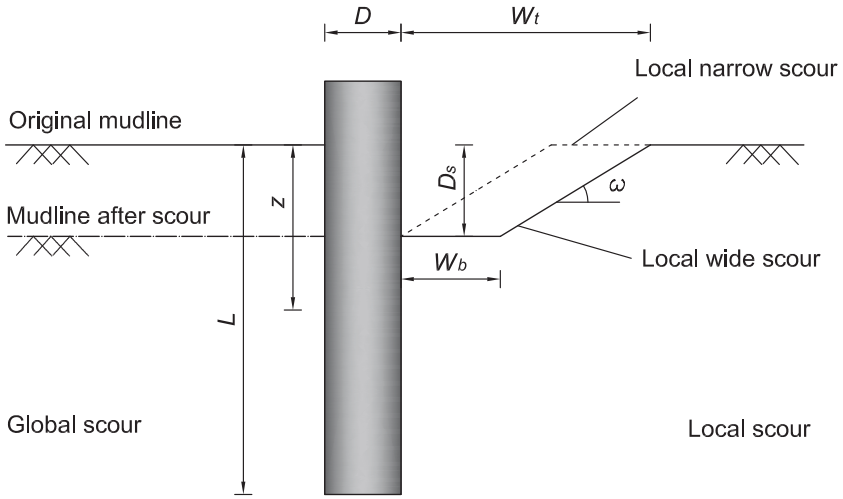

Table 1. Model and corresponding prototype pile dimensions and properties (centrifuge tests were performed at 100*g*).

Property	Model pile	Prototype pile*
Length (embedded + load eccentricity)	90 + 144 mm	9 + 14.4 m
Diameter, outer	18 mm	1.8 m
Wall thickness	1 mm	30 mm*
Elasticity modulus, *E*	70 GPa	210 GPa*
Moment of inertia, *I*	1936 mm^4	0.065 m^4
Bending stiffness, *EI*	0.137 kPa·m^4	13.7 GPa·m^4

*Assuming prototype pile is fabricated from steel.

et al. (2010), Mostafa (2012), Qi et al. (2016), and Zhang et al. (2017) suggested that the assumption of a global scour can be highly conservative. Similarly, centrifuge tests on piles with *L*/*D* = 12.7 conducted by Qi et al. (2016) indicated that removing the entire soil layer to the scour depth can result in a 49%–68% increase in lateral displacement of the pile at a fixed load, when compared to a model where three-dimensional scour-hole dimensions were incorporated. A more realistic approach is to consider a three-dimensional shape for a scour hole. In an attempt to follow the second modelling approach, Lin et al. (2014) developed simplified stiffness models for soil reaction based on the Winkler model (*p*–*y* (soil reaction – displacement) curves) assuming a wedge failure mechanism for a slender laterally loaded pile (*L*/*D* = 35) subjected to scour. Their model was verified with a three-dimensional finite element model. The pile response accounted for both the scour-hole geometry and the overconsolidation effects of the removed soil on the remaining soil. It was found that for global scour, the *p*–*y* curves at given depths were essentially identical when comparing between those below the post-scour surface and those at the same depths without scour. In contrast, for local scour, the *p*–*y* response at a given depth was found to be much stiffer below the scour-hole base than at the same depth below the original soil surface. Lin et al. (2014) concluded that the difference in the effects of global and local scour is attributed to the beneficial influence of the remaining overburden soil surrounding the pile in the latter case.

To address the dearth in experimental data concerning the impact of scour-hole geometry on the response of rigid monopiles, this paper presents the results of a series of centrifuge model tests that were conducted considering different parameters, such as scour depth and scour-hole dimension as well as the magnitude of applied lateral and moment loading. Based on the measured bending moment distributions, *p*–*y* curves were derived and analysed to evaluate the impact of scour type on the tested piles. Using this analysis of experimental data, a new design method has been developed to take the three-dimensional shape of the scour hole into account. An example of the design method is presented in Section 4.3 of the paper.

Fig. 2. Model pile schematic diagram with strain gauge layout (dimensions in millimetres).

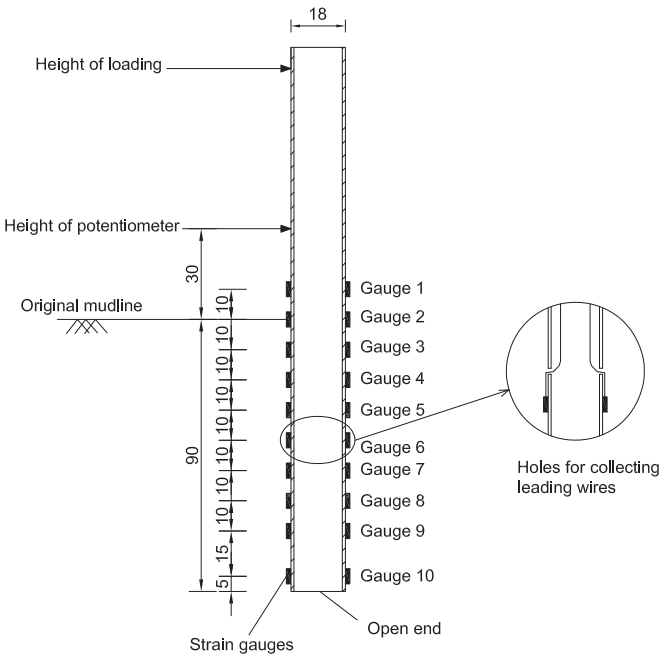

Table 2. Soil properties of Geba sand (De Jager et al. 2017; Maghsoudloo et al. 2018).

e_{min}	e_{max}	G_s	D_{50} (mm)	C_U	φ_{cr}
0.64	1.07	2.67	0.11	1.55	35°

2. Experimental set-up

2.1. Model pile and soil characterisation

The model pile was open-ended and fabricated from a hollow, circular, aluminium tube with an outer diameter (*D*) of 18 mm and an embedment length (*L*) of 90 mm. Therefore, an *L*/*D* ratio of

Fig. 3. Two-dimensional loading actuator and pile testing set-up: (*a*) schematic diagram and (*b*) photo. [Colour online.]

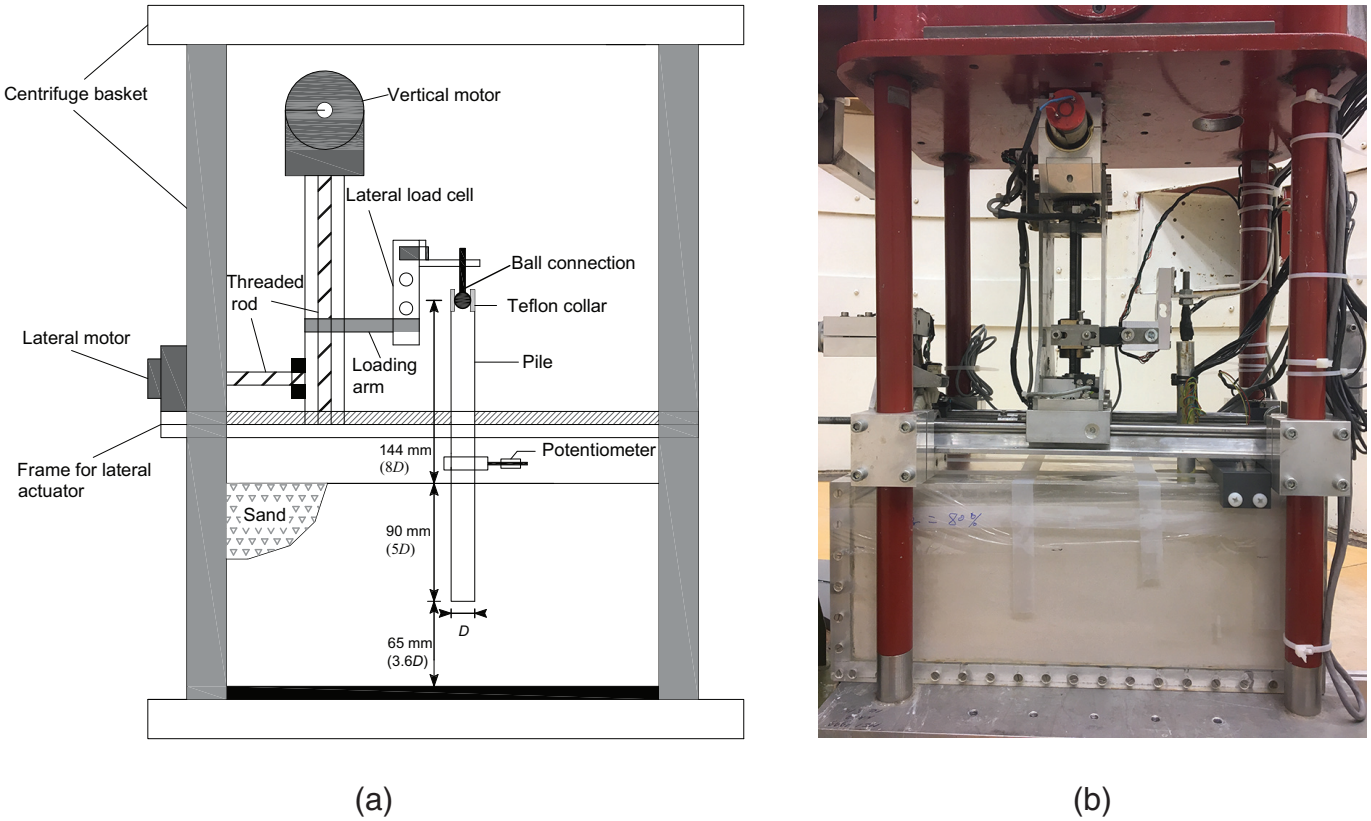

5 was achieved, which is in good accordance with those typically used in the offshore environment. The pile diameter is selected to minimize boundary effects associated with the centrifuge strongbox, which houses the pile, and to satisfy constraints associated with the mean grain particle size. Certainly, the pile in this research has a small diameter with respect to those typically used in the offshore environment (Arany et al. 2017; Prendergast et al. 2018). However, the pile L/D ratio was closely simulated between offshore monopile applications and the model pile in this study.

The pile wall thickness (t) was derived based on the calculations for minimum wall thickness for monopiles (API 2007; Arany et al. 2017; Li et al. 2020). Byrne et al. (2015) produced a database of piles and presented that the pile diameters normalized to pile wall thickness varied from 39 to 80. In the present analysis, the D/t value is 60, suggesting this pile has a good rigidity (in line with present developments for offshore wind monopile foundations). Aluminium was selected as the material to fabricate the pile, therefore the pile wall thickness could be enlarged while the flexural rigidity was kept the same to satisfy the scaling laws. The primary dimensions and material properties of the pile can be found in Table 1. The scaling factor in length is set as 0.01. The pile was instrumented with 10 levels of strain gauges calibrated for measuring bending moment (see Fig. 2). The model pile was jacked into the sand sample prior to spinning up the sample (i.e., installation at 1*g*) with the result that installation effects were not fully modelled. However, the same preparation method and testing procedure was followed for all the tests.

The experiments were conducted using dry Geba silica sand. The mechanical parameters for Geba sand have been determined by Charles University in Prague at the request of Royal IHC (Masin 2017). The drained triaxial tests have been performed on sand with a relative density (D_r) = 80% up to an axial strain of at least 20% (~17.7% shear strain) under confining pressures of 50, 100, and 150 kPa. The critical (post-rupture) shear strength was measured as $\varphi_{cr} = 35°$. The geotechnical characteristics of the sand are summarized in Table 2. The D_r of the prepared sand specimens in tests was 80%.

2.2. Centrifuge loading actuator

The experiments were performed using the beam centrifuge in the Geo-Engineering Section of TU Delft (Allersma 1994; Zhang and Askarinejad 2019). A two-dimensional actuator, which is shown in Fig. 3, was used to impose lateral load (H) at the pile head. Applied lateral load was measured by parallel beam load cell (HTC-SENSORS; TAL220; measuring range 100 N; sensitivity 0.05%). Pile lateral displacements were measured at two locations: pile top using the signal encoder of the actuator, and 1.7D above the sand surface using a potentiometer (ETI SYSTEMS; LCP8S-10; measuring range 0–14 mm; sensitivity 0.2%). These two measurements facilitate the calculation of both lateral translation and rotation of the model pile. A specially designed friction-reducing ball connection was constructed to transfer the lateral loading with application of minimal rotational constraint at the pile top. Details of this ball connection are described by Li et al. (2020) and Chortis et al. (2020).

In the following, the experimental data are expressed in prototype scale. For all tests performed in this study, the centrifuge acceleration level was 100*g*. Lateral loading was applied at a predetermined height $e = 8D$ above the original sand surface, to mimic the lateral loading and significant overturning moment resulting from combinations of wind, wave, and current actions. The pile diameter was 1.8 m and original embedment depth was 9 m ($L/D = 5$).

2.3. Scour-hole formation

A certain scour hole could be determined by scour shape, scour depth, and scour-hole slope angle. Using the scour bottom width

Fig. 4. Schematic illustration of (*a*) local narrow scour, (*b*) local wide scour, and (*c*) global scour (dimensions in metres).

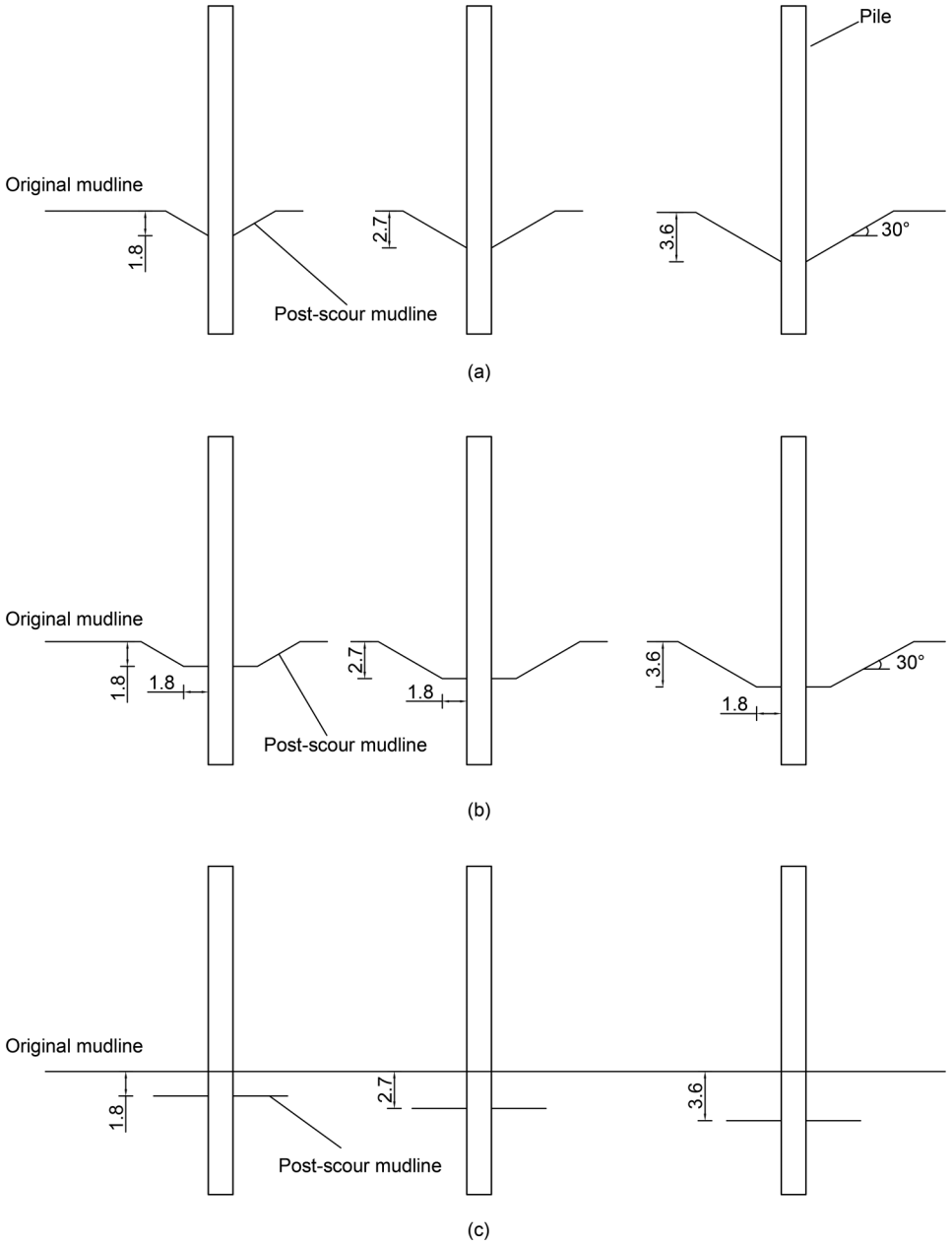

(W_b) for differentiating local narrow scour and local wide scour, the value of 0 and D were chosen in accordance with Mostafa (2012). It has been documented that local scour depth in sandy soils (D_s) is 1.3 times pile diameter (D) with a mean of 0.7 (Sumer et al. 1992). Moreover, the maximum scour depth is reported to be about 2 times the pile diameter (i.e., $D_s/D = 2$). Global scour exposing piles due to storm surge events has been reported in the literature (Robertson et al. 2007) where the ultimate scour depth ratio (D_s/D) is 0.75 to 1. This study focused on scour depths from 1D to 2D, which covers the common scour depth range and, more importantly, the critical value of scour depth that a wind turbine will most likely experience. Scour-hole slope angle was found to be the least important factor among the three scour-hole geometry parameters (scour type, scour depth, and scour-hole slope angle) influencing the responses of laterally loaded piles (Li et al. 2013). Zhang et al. (2017) indicated that an increase of the scour-hole slope angle from 20° to 60° only results in a decrease of the pile-head deflection and maximum bending moment by approximately 5% and 2.5%, respectively, when $D_s = 4D$ and $W_b = 0$. Lin et al. (2016) observed that for a case with $D_s = 3D$ and $W_b = 0$, changing the slope angle from 0° to 60° reduced the maximum bending moment by only 6%–8%. Li et al. (2013) investigated the influence of scour slope angle on the pile-head lateral load versus lateral deflection relationship. They found that when the slope angle was larger than 13°, the pile-head lateral load versus lateral deflection curves at different scour slope angles (13°, 24°, 33°, 45°, 90°) overlap each other. This suggests that the effect of the scour-hole slope angle on the lateral response of the pile is not as significant when the slope angle is >13°.

Therefore, to cover the main range of expected scour-hole geometries, three scour depths: 1.8 m (1D), 2.7 m (1.5D), and 3.6 m (2D); and three scour shapes: local narrow scour, local wide scour,

Table 3. Parameters for centrifuge tests.

Test name	D_r (%)	Scour type	Scour depth
S–NS	80	NS	—
S–LN-1*D*	80	LN	1*D*
S–LN-1.5*D*	80	LN	1.5*D*
S–LN-2*D*	80	LN	2*D*
S–LW-1*D*	80	LW	1*D*
S–LW-1.5*D*	80	LW	1.5*D*
S–LW-2*D*	80	LW	2*D*
S–GL-1*D*	80	GL	1*D*
S–GL-1.5*D*	80	GL	1.5*D*
S–GL-2*D*	80	GL	2*D*

Note: NS, no scour; LN, local narrow; LW, local wide; GL, global.

and global scour, were modelled (Li et al. 2020) (schematically shown in Fig. 4). Global scour was modelled by removing the soil layer of thickness equal to different scour depths. For the tests with local scour, scour holes were created in the shape of inverted circular cones. To compare the influence of scour-hole shape, the scour-hole base extended around the pile at a distance varying between 0 and D (shown as W_b in Fig. 1). Local narrow scour was defined when the scour-hole base had a dimension $W_b = 0$. When the scour-hole base had a dimension $W_b = D$, it was named local wide scour. The scour-hole slope angle was kept constant at 30°, which is in line with the experimental investigation of Roulund et al. (2005) and recommendation of Hoffmans and Verheij (1997). The scour holes were formed after sand specimen preparation using a grab bucket, and each hole was checked using specifically fabricated moulds.

2.4. Testing programme

Following the creation of a scour hole (when relevant), each pile was pushed into the given soil location at 1g using the vertical actuator operating at a rate of 0.1 mm/s to the target depth of $L = 5D$. Subsequently, the model was subjected to an enhanced acceleration field of 100g. The lateral load was applied to the pile-head by the lateral movement of the actuator at a constant rate of 0.02 mm/s.

The testing programme comprised 10 tests: one monotonic load test with no scour (reference test) and nine monotonic load tests with three scour types and three scour depths (see Table 3). The effects of global scour, local narrow scour, and local wide scour were assessed at scour depths of 1*D*, 1.5*D*, and 2*D*.

3. Centrifuge test results

The results of the laboratory tests were investigated by plotting the angular rotation of the pile θ in response to the applied moment M, all measured at the sand surface. Normalizing these parameters enables comparison of results across scales. In this study, M and θ were normalized according to the equations suggested by LeBlanc et al. (2010):

$$(1) \qquad \tilde{M} = \frac{M}{L^3 D \gamma}$$

$$(2) \qquad \tilde{\theta} = \theta \sqrt{\frac{p_a}{L\gamma}}$$

where $\tilde{M}$ is the normalized moment, γ is the sand unit weight, $\tilde{\theta}$ is the normalized pile rotation, and p_a is the atmospheric pressure.

The method for data extraction is outlined in Fig. 5 based on the test data of the no scour case (S–NS). The results indicate that the pile rotation increases continuously as the applied moment increases, thus there is no distinct point that can be used to define failure. Following the recommendation of LeBlanc et al. (2010), failure was defined by $\tilde{\theta}$ = 4° = 0.0698 rad. The moment capacity (M_R) for the pile under the no scour case was determined to be 0.84.

Fig. 5. Determination of moment capacity (test S–NS).

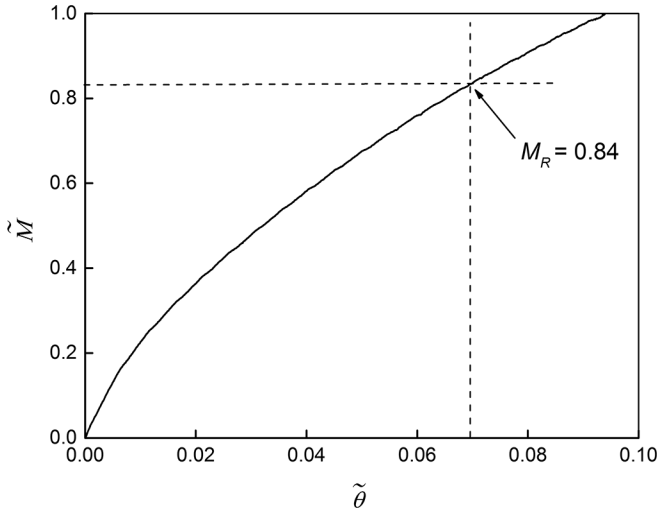

3.1. *p–y* reaction curve construction

Using the strain gauge data, the measured distribution of bending moment $M(z)$, with depth z, was used to derive the soil reaction $p(z)$, by double differentiation, and the displacement profile $y(z)$, by double integration, according to the following equations:

$$(3) \qquad p(z) = \frac{d^2M(z)}{dz^2}$$

$$(4) \qquad y(z) = \iint \frac{M(z)}{EI}\, dz\, dz$$

where $M(z)$ is the bending moment at soil depth z and EI denotes the pile bending stiffness.

The sixth-order polynomial curve-fitting method was adopted to fit the moment data points. It was then differentiated twice, and the soil response $p(z)$ was evaluated.

When determining displacement at any depth, $y(z)$, two integration constants C_1 and C_2 were determined from (*i*) the measured displacement at the loading position and (*ii*) an assumed zero displacement condition at the point with zero lateral soil resistance (Wang and Qi 2008).

The measured bending moment (M) distributions, corresponding deduced distributions of soil resistance (p), and lateral pile displacement (y) for test S–NS are shown in Fig. 6. It can be seen that, with increasing lateral load, the bending moment, soil resistance, and pile lateral displacement all increase. The results generally suggest rigid pile behaviour, with significant displacement of the pile tip developed opposite to the loading direction.

The *p–y* curves were obtained by combining the soil resistance (p) and lateral displacement (y) at discrete intervals to produce curves at each depth, as shown in Fig. 7. Absolute values are plotted, noting that the curves at depths of 7, 8.5, and 9 m correspond to passive soil pressures (negative values of displacement). The stiffness of the *p–y* curves increases rapidly with soil depths for $z \leq 4$ m, whereas the difference between the *p–y* curves on the passive side also appears quite significant ($z \geq 7$ m).

3.2. Effect of scour type on the lateral pile behaviour

The effect of the scour type, i.e., global, local wide, and local narrow scour around the monopile, on the lateral behaviour of the foundation is discussed from three aspects: (*i*) moment–rotation

Fig. 6. Distributions of (*a*) measured bending moment; (*b*) lateral soil resistance; (*c*) lateral pile displacement under different values of applied moment (test S–NS).

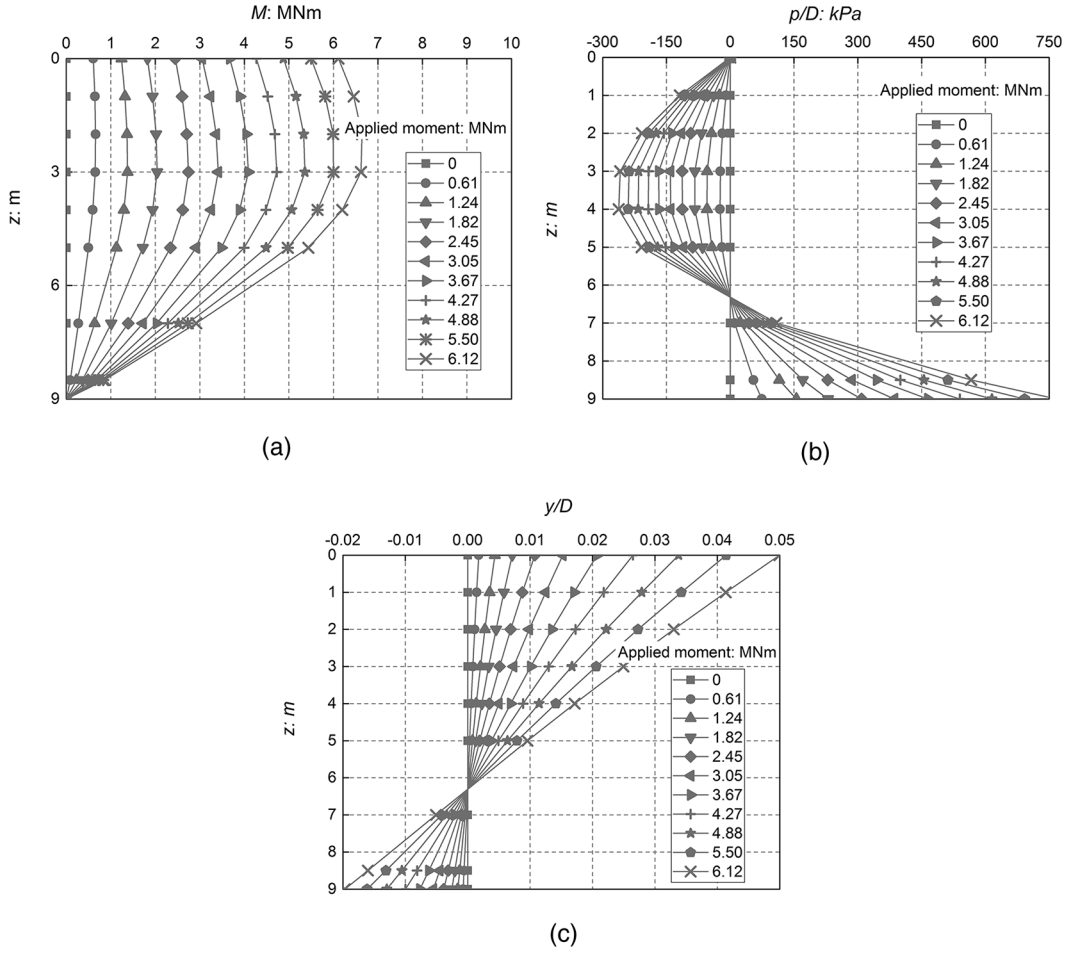

at the sand surface, (*ii*) distribution of bending moment along the pile, and (*iii*) soil reaction curves (*p*–*y* curves)

3.2.1. Moment–rotation behaviour

Figure 8 shows the moment–rotation curves from centrifuge tests considering different scour types and scour depths. In all figures, the pile with no scour shows the highest initial stiffness and capacity, followed by local narrow scour, local wide scour, and global scour. Comparing the measurements from the local wide and global scour cases, results suggest that the remaining soil above the scour baseline can have considerable effect on the confining stresses and hence on the lateral stiffness of the foundation system. The difference in pile stiffness and capacity between local narrow and local wide scour may be due to the difference in the amount of soil above the scour baseline.

As suggested by DNV (2016), the typical limiting rotation is 0.5° at the soil surface, whereas a 0.25° construction tolerance should be taken into account. Therefore, an allowable accumulated rotation (AAR) is 0.25° due to various types of loading during the life time of OWTs (Truong et al. 2019), which corresponds to $\tilde{\theta}_{AAR}$ = 0.00375 rad. From Fig. 8 it can be seen that, at scour depths of 1*D* and 1.5*D*, scour type has minimal effect on the initial stiffness of pile lateral bearing behaviour, which suggests that when performing pile dynamic analysis within a small strain range, scour type can be regarded as having no effect, especially at shallow scour depths ($D_s < 1.5D$). At very large scour depths (2*D* for example), effect of scour type should certainly be taken into consideration, as the initial stiffness of the pile is significantly influenced by scour type.

Fig. 7. Experimental *p*–*y* curves at different soil depths (test S–NS).

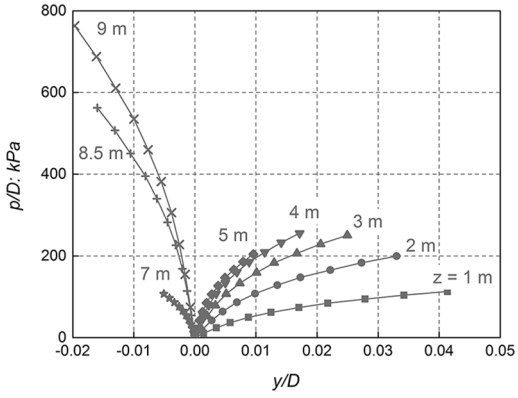

Moment reduction factor, $M_{R,reduction}$, is used to describe the influence of scour on the moment capacity, which is defined in the following equation:

$$M_{R,reduction} = \frac{M_{R,no\ scour} - M_{R,with\ scour}}{M_{R,no\ scour}} \quad (5)$$

where $M_{R,reduction}$ denotes the reduction of M_R as a result of scour, $M_{R,no\ scour}$ is the moment capacity under no scour conditions,

Fig. 8. Influence of scour type on the moment–rotation response of piles: (*a*) scour depth 1*D*, (*b*) scour depth 1.5*D*, and (*c*) scour depth 2*D*. [Colour online.]

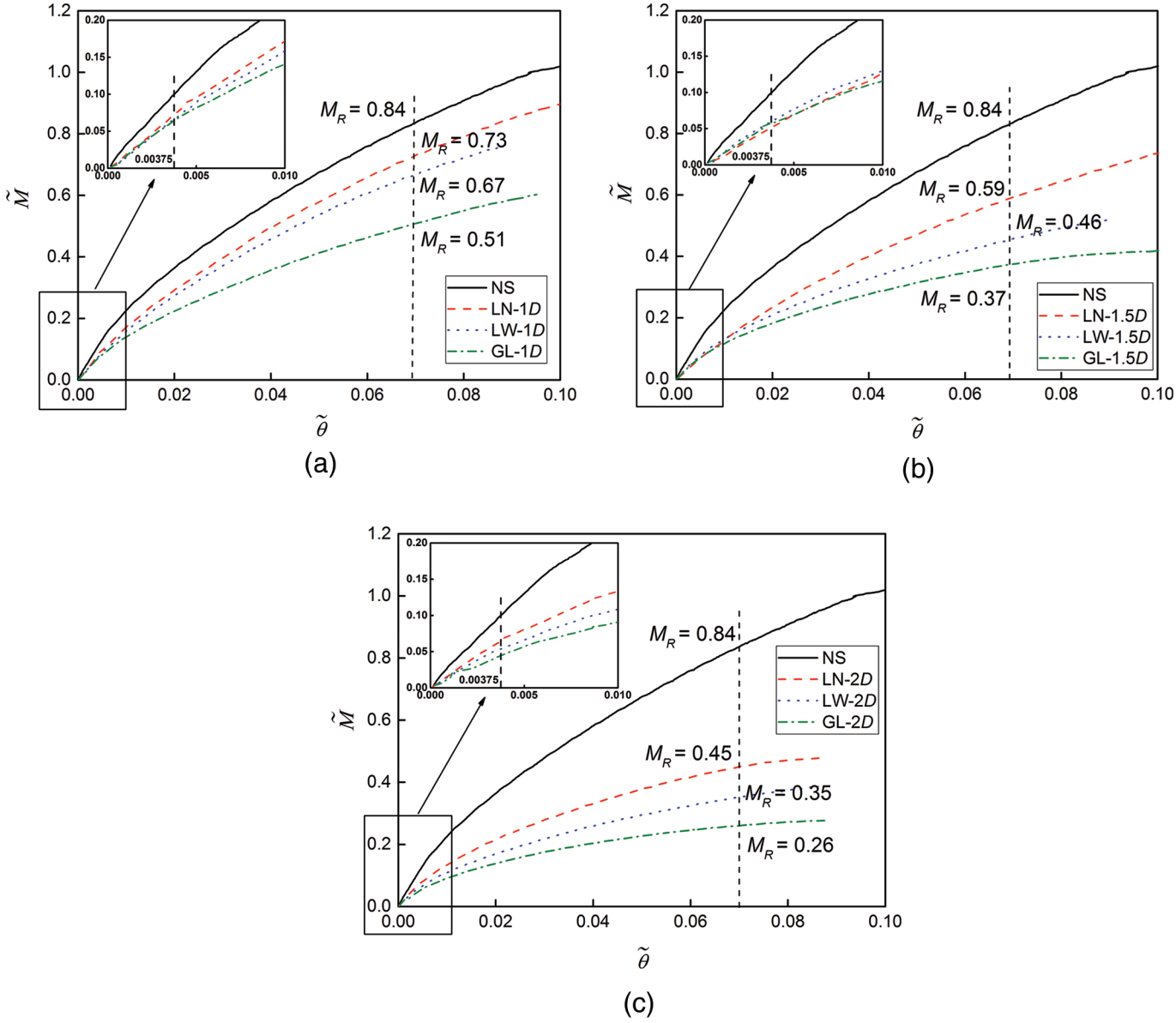

and $M_{R,\text{with scour}}$ is the moment capacity under scour conditions. The reduction of moment capacity compared with the reference case, which increases with scour depth, can be seen in Table 4, which shows reduction of 13%–39% for a scour depth of 1*D*, increasing to 46%–69% for a scour depth of 2*D*.

Table 4. Reduction of moment capacity ($M_{R,\text{reduction}}$) as a result of scour.

Scour type	$D_s = 1D$	$D_s = 1.5D$	$D_s = 2D$
Local narrow scour	0.13	0.30	0.46
Local wide scour	0.20	0.45	0.58
Global scour	0.39	0.56	0.69

3.2.2. Bending moment distributions

The normalized bending moment profiles of piles subjected to an external normalized bending moment of $\tilde{M} = 0.2$ under various types and depths of scour are shown in Fig. 9. For all scour types and depths considered, the bending moment along the pile increased significantly compared to the no scour case. This would suggest in practice that an increase of pile diameter and (or) wall thickness might be required during design of a monopile installed in an area with potential of scour (Arany et al. 2017). For scour depths of 1*D* and 1.5*D*, the moment profiles developed for local wide scour and global scour are very similar, and those for the case of local narrow scour are slightly smaller. Therefore, it can be concluded that scour shape has no significant effect on the bending moment profile along the embedded length of the pile at a shallow scour depth ($D_s \leq 1.5D$). However, there is a clear distinction between results of scour types as scour depth increased to 2*D*, due to the enlarged difference in the overburden pressure above scour baseline. Local narrow scour has the highest amount of overburden pressure, followed by local wide scour, then global scour. The decrease in the overburden pressure caused a decrease in the vertical and lateral effect stresses in the soil below the scour baseline. As a result, the soil resistance and pile capacity decreased and pile bending moment increased.

Fig. 9. Profiles of bending moment along the pile at various scour types ($\tilde{M}$ = 0.2): (*a*) scour depth 1*D*, (*b*) scour depth 1.5*D*, and (*c*) scour depth 2*D*. [Colour online.]

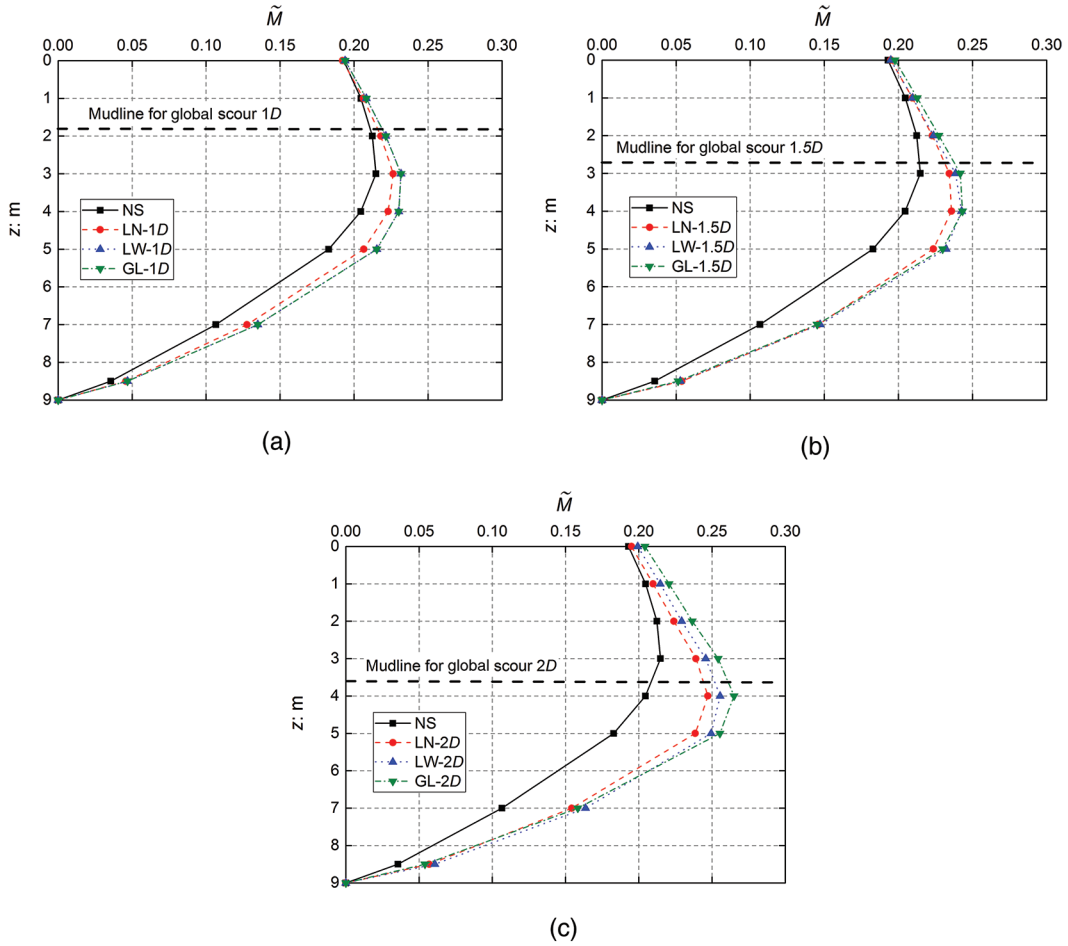

3.2.3. *p–y* reaction curves

The *p–y* curves at a soil depth of *z* = 3 m are compared for different shapes of scour with depth of 1*D* in Fig. 10. The results indicate that the no scour case shows the highest soil reaction at this depth for any level of pile lateral displacement. Moreover, it can be observed that the soil elements around the piles experiencing a 1*D* scour condition show much lower stiffness comparing to the intact soil surface situation. The difference in the *p–y* curves between the cases of local wide and global scour conditions is not that significant compared with no scour and local narrow scour conditions.

The effects of scour shape and depth on the *p–y* curves for various depths below the original mudline level are illustrated in Fig. 11. It can be concluded that at scour depths of 1*D* and 1.5*D* the *p–y* curves are less sensitive to the scour shape. Similarly, for a scour depth of 2*D* the initial response ($y/D < 0.005$) of *p–y* curves is not significantly affected. This observation implies that the dynamic behaviour of the pile at small strains might not be affected by the scour shape. However, at larger strains the pile under local narrow scour mobilizes the highest amount of soil resistance, followed by local wide scour, then global scour. This observation might be due to the fact that the major consequential difference between local narrow scour and local wide scour is the amount of overburden pressure and resistance provided by the sand slope near the pile, while the difference between local wide scour and global scour lies in the overburden pressure provided by the soil above the scour base mudline.

Fig. 10. *p–y* curves at *z* = 3 m in the cases of no scour, 1*D* local narrow scour, 1*D* local wide scour, and 1*D* global scour. [Colour online.]

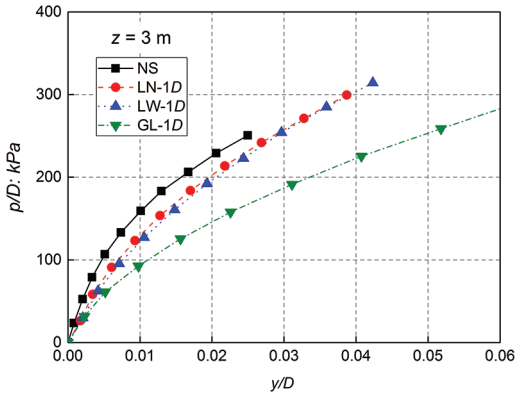

3.3. Effect of scour depth on the moment–rotation behaviour of the monopile

Figure 12 shows the influence of scour depth on the rotation of monopiles subjected to a certain external bending moment of $\tilde{M}$ = 0.2. The results indicate that for all three scour types, $\tilde{\theta}$ increases significantly with the increase of scour depth. For example, the rotation of the pile can be increased by a factor of 3.48 in the case of a global scour condition with a depth of 2*D*. By interpolating data when scour depth $D_s \in [0, 1D)$, the

Fig. 11. *p*–*y* curves at z = 4 m for different scour types: (*a*) scour depth 1*D*, (*b*) scour depth 1.5*D*, and (*c*) scour depth 2*D*.

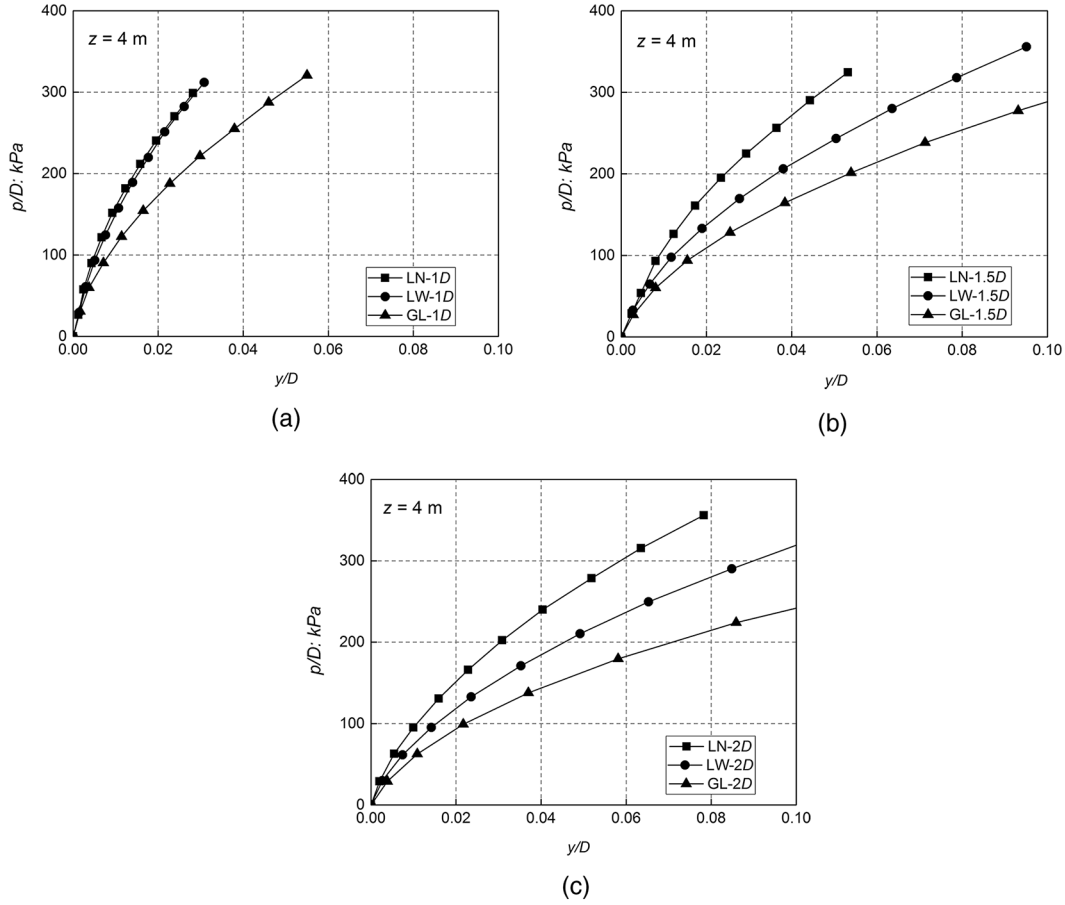

difference of normalized pile rotation among scour types of local narrow, local wide, and global at the scour depth $D_s/D = 0.5$ is not significant.

The effects of scour depth on the moment capacity of laterally loaded piles subjected to various types of scour are shown in Fig. 13. The results indicate that for all three scour types, $\tilde{M}$ decreases almost linearly with the increase of scour depth. The rate of this increase has a direct relationship with the amount of pile normalized rotation, $\tilde{\theta}$.

Under various kinds of scour types, the decrease of pile capacity due to the increase of scour depth could be directly related to the loss of overburden pressure. As mentioned in the previous section, a decrease in the overburden pressure leads to a decrease in the vertical and lateral effect stresses in the soil underneath. Therefore, the soil resistance and pile capacity decreased, while the pile bending moment increased.

4. Discussion and new design method

Based on the centrifuge tests results, a new design method was developed to consider the three-dimensional shape of the local scour holes around the monopile. Section 4.1 will discuss the basics of the method by introduction of an equivalent scour depth according to the shape of the local scour. The steps of the proposed method are presented for a case study in Section 4.2.

4.1. Equivalent scour depth z_{equ}

The results from the centrifuge tests indicate that the detrimental effects of scour are generally less in cases of local scour compared with those of global scour. Therefore, as a practical

Fig. 12. Influence of scour depth on the normalized pile rotation ($\tilde{M}$ = 0.2). [Colour online.]

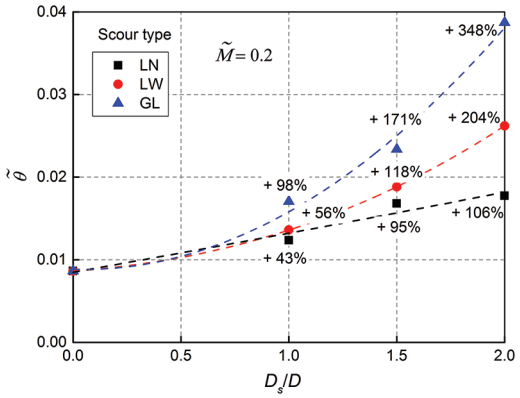

approach to account for the effect of local scour types compared with global scour on the pile moment capacity, the term additional soil depth (z_{add}) is introduced and is defined in eq. 6. In this approach, the beneficial effect of local scour types is deemed as an additional soil layer lying above assumed global scour, which leads to a larger pile embedment length after local scour (L) and a smaller loading eccentricity (e), as illustrated in Fig. 14. In this figure, the terms $z_{add,LN}$ and $z_{add,LW}$ denote additional soil depth to account for local narrow scour (LN) and local wide scour (LW) scour types, respectively. Another term, equivalent scour depth (z_{equ}), is introduced hereafter, which signifies the effective

Fig. 13. Influence of scour depth on the moment bearing: (*a*) local narrow scour, (*b*) local wide scour, and (*c*) global scour. [Colour online.]

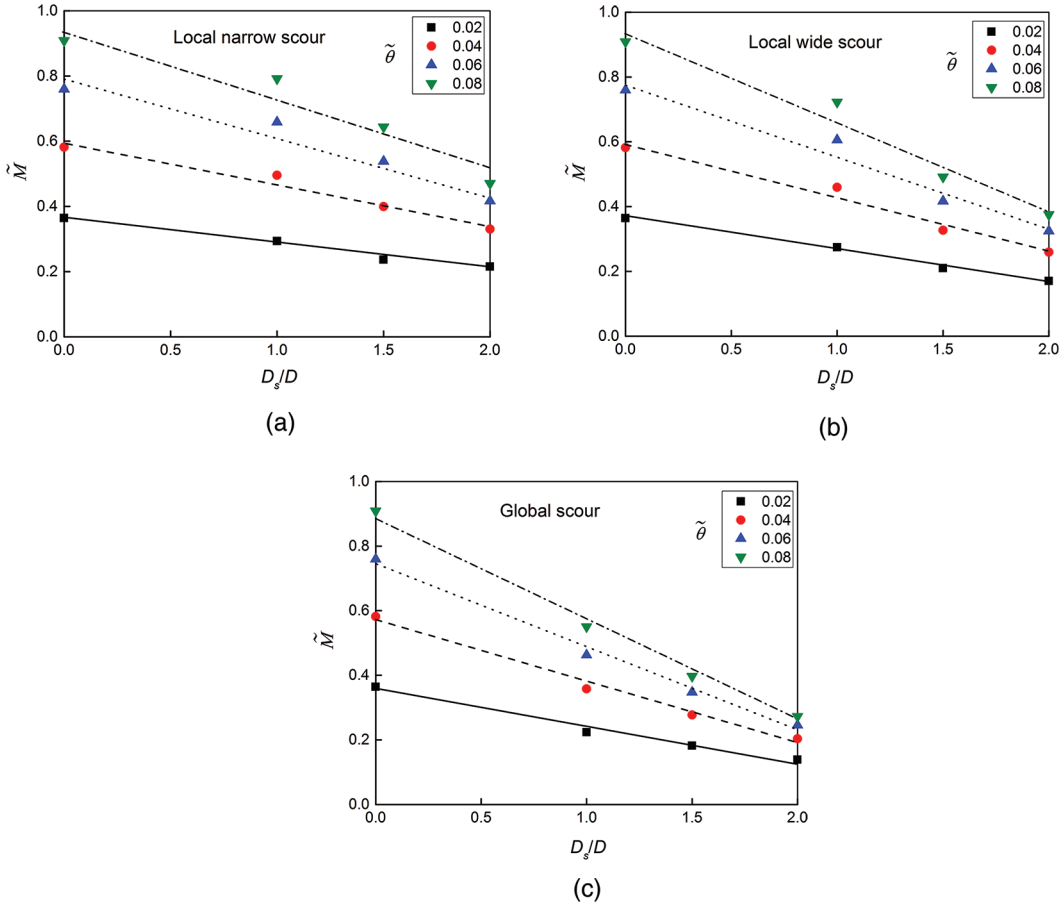

Fig. 14. Illustration of the additional soil depth (z_{add}).

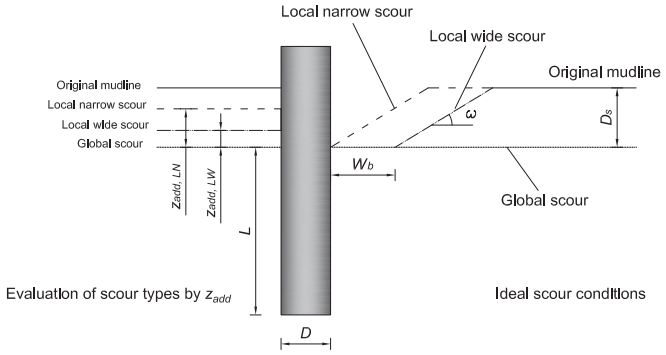

scour depth after taking into account the compensation effect by local scour types compared with global scour, which is defined by eq. 7.

$$z_{add} = \delta D_s \quad (6)$$

$$z_{equ} = D_s - z_{add} = D_s(1-\delta) \quad (7)$$

Compared with global scour, the improvement in moment capacity by local scour types is quantified by the additional soil depth factor, δ. Therefore, the condition of global scour is set as the base level for δ, i.e., no compensation effect is introduced that corresponds to $\delta = 0$. Consequently, the condition of no scour can be set as the upper boundary for δ and it can be considered as full compensation, which corresponds to $\delta = 1$. Thus, δ for the local scour types ranges between 0 and 1.

Table 5. Equivalent scour depth (z_{equ}).

Scour type	$D_s = 1D$	$D_s = 1.5D$	$D_s = 2D$
Local narrow scour	0.34*D*	0.87*D*	1.3*D*
Local wide scour	0.67*D*	1.215*D*	1.66*D*
Global scour (= D_s)	1*D*	1.5*D*	2*D*

Figure 15 shows the influence of scour type on the normalized external moment at various scour depths, along with the strategy to determine the additional soil depth factor (δ) experimentally. For example, for 1*D* local narrow and 2*D* local wide scour conditions, δ would be equal to 0.66 and 0.17, respectively. This means that the equivalent scour depths for these two cases are 0.34*D* and 1.66*D*, respectively. The equivalent scour depths for various conditions are summarized in Table 5.

As a practical approach to incorporate effects of scour type on equivalent scour depth (z_{equ}), the data from Table 5 were used to plot the relationship between z_{equ}/D and D_s/D considering different scour types, as shown in Fig. 16. When the scour depth $D_s \in [1D, 2D]$, linear fits between z_{equ}/D and D_s/D were found and the following empirical equation was generated:

$$\frac{z_{equ}}{D} = \frac{D_s}{D} - f \quad (8)$$

In this equation, $f = 0$, for global scour; $f = 0.4$, for local wide scour; $f = 0.7$, for local narrow scour.

Fig. 15. Determination of the additional soil depth factor (δ): (*a*) scour depth 1*D*, (*b*) scour depth 1.5*D*, and (*c*) scour depth 2*D*. [Colour online.]

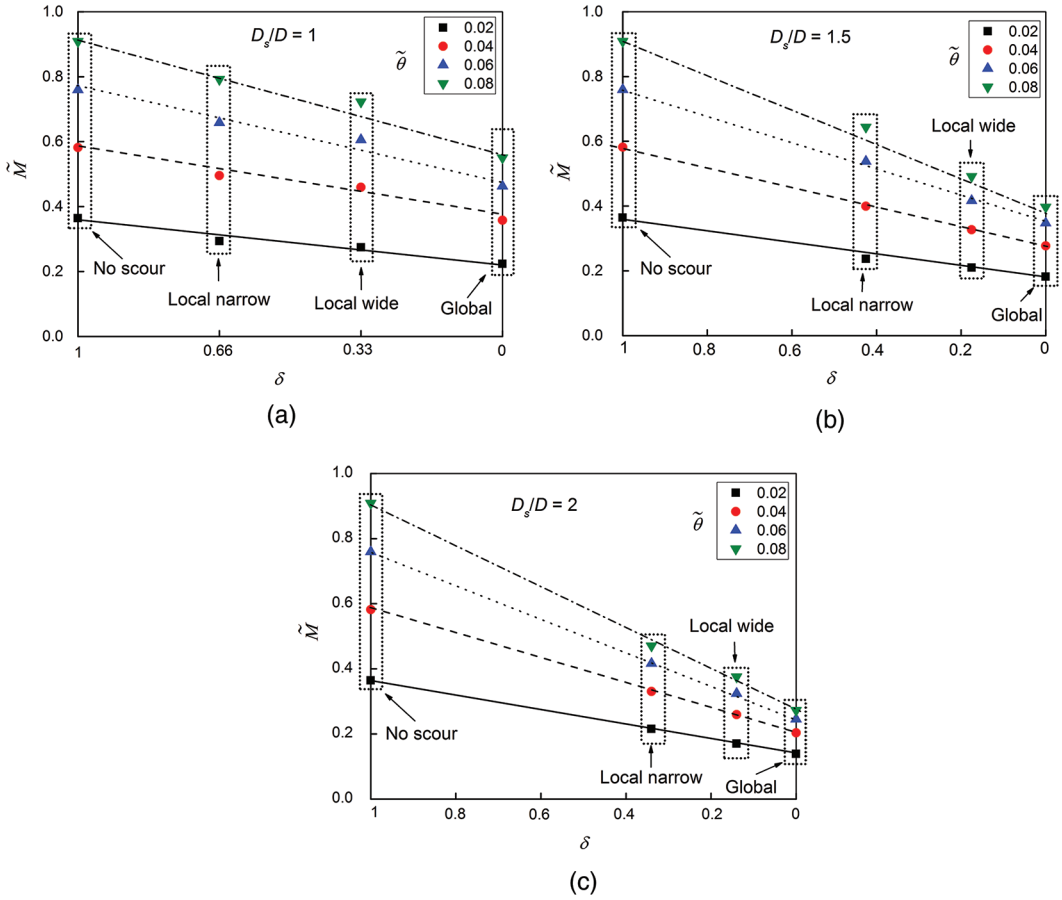

However, when the scour depth $D_s \in [0, 1D)$, the effect of scour type is not significant on the pile rotation (Fig. 12). Therefore, as a preliminary attempt linear interpolation technique could be applied which leads to the following empirical equation:

$$\frac{z_{equ}}{D} = \frac{D_s}{D}(1 - f) \quad (9)$$

In this way, the beneficial effect of local scour shapes can be practically considered as shallower global scours, when designing the pile foundation from a moment capacity perspective. The derived empirical equation offers a straightforward approach to calculate the equivalent scour depth (z_{equ}).

4.2. Reduction of pile moment capacity caused by scour

The data from Table 4 were used to plot the relationship between $M_{R,reduction}$ and scour depth (D_s) considering different scour types, which is shown in Fig. 17. When the scour depth $D_s \in [1D, 2D]$, a linear equation was used to fit the data, resulting in the following general equation:

$$M_{R,reduction} = 0.35\frac{D_s}{D} + r \quad (10)$$

In this equation, r is a fitting parameter and is equal to 0.05, –0.16, and –0.2 for global scour, local wide scour, and local narrow scour, respectively.

Similar to the technique in the derivation of equivalent scour depth (z_{equ}) when the scour depth $D_s \in [0, 1D)$, the linear interpolation technique could be applied, which leads to the following empirical equation:

$$M_{R,reduction} = \frac{D_s}{D}(0.35 + r) \quad (11)$$

Using this method, the detrimental influence of scour on the moment capacity can be directly related to the scour depth and scour type. In the practical application, depending on the formation of the scour hole, as long as the scour type and scour depth

Fig. 16. Influence of scour type on the equivalent scour depth (z_{equ}). [Colour online.]

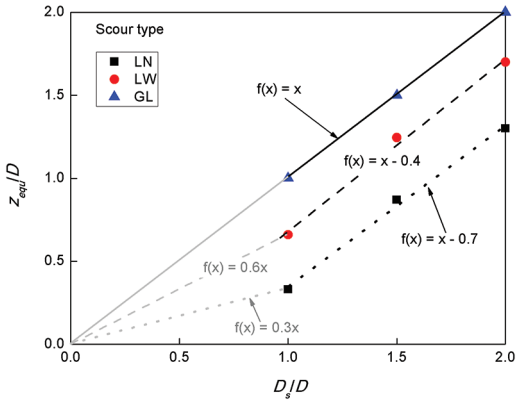

Fig. 17. $M_{R,reduction}$ versus D_s/D. [Colour online.]

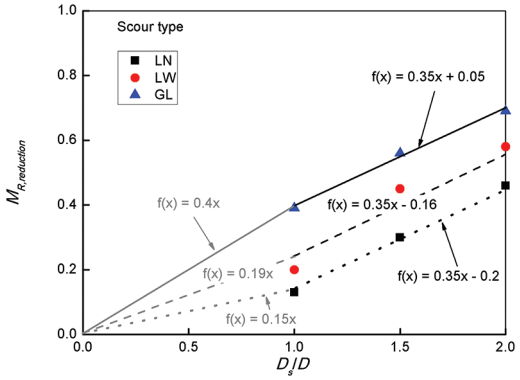

are primarily estimated, the moment capacity reduction factor $M_{R,reduction}$ can be estimated from Fig. 17, and then be employed by the following equation to determine the design pile moment capacity under scour condition ($M_{R,with\ scour}$):

$$M_{R,with\ scour} = M_{R,no\ scour}(1 - M_{R,reduction}) \quad (12)$$

In this equation, $M_{R,with\ scour}$ is the design pile moment capacity considering the influence of scour and $M_{R,no\ scour}$ is the design pile moment capacity when no scour erosion is considered.

4.3. Example

An example is given to demonstrate the use of the proposed equivalent scour depth method in this section. Consider a rigid monopile, with L/D = 5, driven into sand with a relative density of 80%. The task is to determine the equivalent scour depth (z_{equ}) and the design pile moment capacity under scour conditions ($M_{R,with\ scour}$) from the equivalent moment capacity point of view, when the pile is subjected to local wide scour with a scour depth of 1.2D. The design pile moment capacity when there is no scour erosion is denoted by $M_{R,no\ scour}$.

According to Fig. 16 the non-dimensional coefficient f, under local wide scour conditions, is 0.4. Therefore, z_{equ} can be calculated using eq. 8:

$$\frac{z_{equ}}{D} = \frac{D_s}{D} - f = \frac{1.2D}{D} - 0.4 = 0.8 \quad (13)$$

This result indicates that local wide scour with a scour depth of 1.2D is equivalent to global scour with a scour depth of 0.8D.

According to Fig. 17 the non-dimensional coefficient r, under local wide scour conditions, is −0.16. Therefore, the moment capacity reduction factor ($M_{R,reduction}$) can be calculated from eq. 10:

$$M_{R,reduction} = 0.35\frac{D_s}{D} + r = 0.35 \times 1.2 - 0.16 = 0.26 \quad (14)$$

Accordingly, the design pile moment capacity under this specific scour condition ($M_{R,with\ scour}$) can be calculated according to eq. 12:

$$M_{R,with\ scour} = M_{R,no\ scour}(1 - M_{R,reduction}) = 0.74M_{R,no\ scour} \quad (15)$$

In summary, the equivalent scour depth is 0.8D and the moment capacity of the pile would decrease by 26% in the case of a local wide scour to a depth of 1.2D.

5. Conclusions

As a process of soil erosion, scour broadly occurs around offshore wind turbine monopiles, which decreases the pile capacity and stiffness and might potentially lead to failure of the structure. A series of centrifuge tests was carried out at 100g on a model monopile installed in dense sand with an embedment ratio of 5 to investigate the effect of scour on the foundation lateral response. Three scour types (local narrow, local wide, and global) and three scour depths (1D, 1.5D, and 2D) were considered in this investigation, which represent a range of common scour shapes in real engineering applications. Empirical equations were derived to evaluate the beneficial effect of local scour types compared with the assumption of global scour conditions, and to assess the detrimental effect of increased scour depth on pile moment capacity. The following conclusions can be drawn from this study:

1. Scour type has significant influence on the pile moment–rotation behaviour. Piles under local narrow scour show the highest moment capacity, followed by local wide scour, and global scour conditions. At scour depths of 1D and 1.5D, scour type has minimal effect on the stiffness of the pile at small rotations, which signifies that in pile dynamic analysis within small strain range the effect of scour type could be ignored. However, the results indicate that in the case of a global scour condition to a depth of 2D, negative effect of scour on the stiffness of pile should certainly be taken into consideration.

   At the same soil depth (z) and lateral displacement (y), pile under local narrow scour mobilizes the highest amount of soil resistance (p), followed by local wide scour, then global scour. The major consequential difference between local narrow scour and local wide scour was speculated as the amount of overburden pressure and resistance provided by the sand slope near to the pile, while the difference between local wide scour and global scour was suspected to be due to the overburden pressure provided by the soil above the scour base. According to this hypothesis, the beneficial effect of local scour types could be regarded as additional soil layers lying above global scour. Empirical equations were derived to calculate the equivalent scour depth (z_{equ}), which can be implemented in the current monopile foundation design methodology.
2. The pile moment capacity was found to decrease almost linearly with the increase of scour depth, in all the three scour types (local narrow scour, local wide scour, and global scour). The pile initial stiffness decreased with increasing scour depth as well. Increasing scour depth leads to an increase in the peak bending moment and moves the location of the peak moment into deeper soil.

   The detrimental effect of scour on the moment capacity, considering the influence of scour depth and scour type, was described by empirical equations for a monopile with L/D = 5 installed in dense sand. In the practical application, depending on the marine hydraulic environment, as long as the type and depth of the scour hole are estimated, the moment capacity reduction factor $M_{R,reduction}$ could be calculated and employed to determine the design pile moment capacity under scour condition ($M_{R,with\ scour}$). In this way, the traditional design method which neither fully considers the effect of scour shape nor properly addresses the effect of scour depth, could be improved.

Acknowledgements

This work is partly funded by the Section of Geo-Engineering, Delft University of Technology. The first author is grateful for the support by the China Scholarship Council (CSC).

References

Allersma, H. 1994. The University of Delft geotechnical centrifuge. *In* Proceedings of the International Conference Centrifuge 94, Singapore, 31 August–2 September 1994. Vol. 94. pp. 47–52.

API. 2007. RP2A: Recommended Practice for Planning, Designing and Constructing Offshore Platforms - Working Stress Design. American Petroleum Institute (API), Washington, DC.

Arany, L., Bhattacharya, S., MacDonald, J., and Hogan, S. 2017. Design of monopiles for offshore wind turbines in 10 steps. Soil Dynamics and Earthquake Engineering, **92**: 126–152. doi:10.1016/j.soildyn.2016.09.024.

Byrne, B.W., McAdam, R., Burd, H.J., Houlsby, G.T., Martin, C.M., Gavin, K., et al. 2015. Field testing of large diameter piles under lateral loading for offshore wind applications. *In* Proceedings of the XVI ECSMGE Geotechnical Engineering for Infrastructure and Development. pp. 1255–1260.

Byrne, B.W., Burd, H.J., Zdravkovic, L., McAdam, R.A., Taborda, D.M., Houlsby, G.T., et al. 2019. PISA: new design methods for offshore wind turbine monopiles. Revue Française de Géotechnique, **158**: 3. doi:10.1051/geotech/2019009.

Chortis, G., Askarinejad, A., Prendergast, L., Li, Q., and Gavin, K. 2020. Influence of scour depth and type on *p–y* curves for monopiles in sand under monotonic lateral loading in a geotechnical centrifuge. Ocean Engineering, **197**: 106838. doi:10.1016/j.oceaneng.2019.106838.

De Jager, R.R., Machsoudloo, A., Askarinejad, A., and Molenkamp, F. 2017. Preliminary results of instrumented laboratory flow slides. *In* Proceedings of the 1st International Conference on the Material Point Method (MPM 2017). *Edited by* A. Rohe, K. Soga, H. Teunissen, and B.Z. Coelho. Elsevier, Delft, the Netherlands.

DNV. 2014. Design of offshore wind turbine structures. Offshore Standard DNV-OS-J101. Det Norske Veritas AS, Oslo, Norway.

DNV. 2016. Support structures for wind turbines. DNVGL-ST-0126. Det Norske Veritas AS, Oslo, Norway.

Doherty, P., and Gavin, K. 2012. Laterally loaded monopile design for offshore wind farms. Proceedings of the Institution of Civil Engineers – Energy, **165**(1): 7–17. doi:10.1680/ener.11.00003.

Hoffmans, G.J., and Verheij, H.J. 1997. Scour manual. CRC Press.

Jones, J.S., Kilgore, R.T., and Mistichelli, M.P. 1992. Effects of footing location on bridge pier scour. Journal of Hydraulic Engineering, ASCE, **118**(2): 280–290. doi:10.1061/(ASCE)0733-9429(1992)118:2(280).

Leblanc, C., Houlsby, G., and Byrne, B. 2010. Response of stiff piles in sand to long-term cyclic lateral loading. Géotechnique, **60**(2): 79–90. doi:10.1680/geot.7.00196.

Li, F., Han, J., and Lin, C. 2013. Effect of scour on the behavior of laterally loaded single piles in marine clay. Marine Georesources & Geotechnology, **31**(3): 271–289. doi:10.1080/1064119X.2012.676157.

Li, Q., Prendergast, L., Askarinejad, A., and Gavin, K. 2018. Effect of scour on the behavior of a combined loaded monopile in sand. *In* Proceedings of the 9th European Conference on Numerical Methods in Geotechnical Engineering (NUMGE 2018), Porto, Portugal, 25–27 June 2018. pp. 25–27.

Li, Q., Prendergast, L., Askarinejad, A., Chortis, G., and Gavin, K. 2020. Centrifuge modeling of the impact of local and global scour erosion on the monotonic lateral response of a monopile in sand. Geotechnical Testing Journal, **43**: 20180322. doi:10.1520/GTJ20180322.

Lin, C., Bennett, C., Han, J., and Parsons, R.L. 2010. Scour effects on the response of laterally loaded piles considering stress history of sand. Computers and Geotechnics, **37**(7–8): 1008–1014. doi:10.1016/j.compgeo.2010.08.009.

Lin, C., Han, J., Bennett, C., and Parsons, R.L. 2014. Analysis of laterally loaded piles in sand considering scour hole dimensions. Journal of Geotechnical and Geoenvironmental Engineering, ASCE, **140**(6): 04014024. doi:10.1061/(ASCE)GT.1943-5606.0001111.

Lin, C., Han, J., Bennett, C., and Parsons, R.L. 2016. Analysis of laterally loaded piles in soft clay considering scour-hole dimensions. Ocean Engineering, **111**: 461–470. doi:10.1016/j.oceaneng.2015.11.029.

Maghsoudloo, A., Askarinejad, A., de Jager, R.R., Molenkamp, F., and Hicks, M.A. 2018. Experimental investigation of pore pressure and acceleration development in static liquefaction induced failures in submerged slopes. *In* Proceedings of the 9th International Conference of Physical Modelling in Geotechnics (ICPMG 2018), 17–20 July 2018. CRC Press, London, UK.

Masin, D. 2017. Calibration of sand hypoplastic model on Geba sand data. Internal report issued for Royal IHC. Charles University in Prague, The Netherlands.

Mostafa, Y.E. 2012. Effect of local and global scour on lateral response of single piles in different soil conditions. Engineering, **4**(6): 297–306. doi:10.4236/eng.2012.46039.

Prendergast, L.J., Reale, C., and Gavin, K. 2018. Probabilistic examination of the change in eigenfrequencies of an offshore wind turbine under progressive scour incorporating soil spatial variability. Marine Structures, **57**: 87–104. doi:10.1016/j.marstruc.2017.09.009.

Qi, W., Gao, F., Randolph, M., and Lehane, B. 2016. Scour effects on *p–y* curves for shallowly embedded piles in sand. Géotechnique, **66**(8): 648–660. doi:10.1680/jgeot.15.P.157.

Richardson, E., and Davis, S. 2001. Evaluating scour at bridges. 4th ed. FHWA NHI, 01-001, HEC-18. US Department of Transportation, Federal Highway Administration, Colo.

Robertson, I.N., Riggs, H.R., Yim, S.C., and Young, Y.L. 2007. Lessons from Hurricane Katrina storm surge on bridges and buildings. Journal of Waterway, Port, Coastal, and Ocean Engineering, ASCE, **133**(6): 463–483. doi:10.1061/(ASCE)0733-950X(2007)133:6(463).

Roulund, A., Sumer, B.M., Fredsøe, J., and Michelsen, J. 2005. Numerical and experimental investigation of flow and scour around a circular pile. Journal of Fluid Mechanics, **534**: 351–401. doi:10.1017/S0022112005004507.

Sørensen, S.P.H., and Ibsen, L.B. 2013. Assessment of foundation design for offshore monopiles unprotected against scour. Ocean Engineering, **63**: 17–25. doi:10.1016/j.oceaneng.2013.01.016.

Sumer, B.M., Fredsøe, J., and Christiansen, N. 1992. Scour around vertical pile in waves. Journal of Waterway, Port, Coastal, and Ocean Engineering, ASCE, **118** (1): 15–31. doi:10.1061/(ASCE)0733-950X(1992)118:1(15).

Truong, P., Lehane, B., Zania, V., and Klinkvort, R.T. 2019. Empirical approach based on centrifuge testing for cyclic deformations of laterally loaded piles in sand. Géotechnique, **69**(2): 133–145. doi:10.1680/jgeot.17.P.203.

Wang, J., and Qi, C. 2008. *Py* curves of piles in saturated degradation sands with residual pore water pressures. *In* Proceedings of the 18th International Offshore and Polar Engineering Conference, Vancouver, BC, 6–11 July 2008. International Society of Offshore and Polar Engineers.

Wu, X., Hu, Y., Li, Y., Yang, J., Duan, L., Wang, T., et al. 2019. Foundations of offshore wind turbines: a review. Renewable and Sustainable Energy Reviews, **104**: 379–393. doi:10.1016/j.rser.2019.01.012.

Zhang, W., and Askarinejad, A. 2019. Centrifuge modelling of submarine landslides due to static liquefaction. Landslides, **16**: 1921–1938. doi:10.1007/s10346-019-01200-z.

Zhang, H., Chen, S., and Liang, F. 2017. Effects of scour-hole dimensions and soil stress history on the behavior of laterally loaded piles in soft clay under scour conditions. Computers and Geotechnics, **84**: 198–209. doi:10.1016/j.compgeo.2016.12.008.

List of symbols

C_1, C_2	integration constants
C_U	uniformity coefficient
D	pile diameter
D_{50}	medium particle size
D_r	relative density
D_s	scour depth
E	elasticity modulus
e	loading eccentricity
e_{max}	maximum void ratio
e_{min}	minimum void ratio
f	nondimensional fitting parameter
G_s	specific gravity
GL	global scour
I	moment of inertia
L	pile length
LN	local narrow scour
LW	local wide scour
M	bending moment
$\tilde{M}$	normalized moment
M_R	moment capacity
$M_{R,no\ scour}$	moment capacity under no scour condition
$M_{R,reduction}$	moment reduction factor
$M_{R,with\ scour}$	moment capacity under scour condition
NS	no scour
p	soil reaction
p_a	atmospheric pressure
r	non-dimensional fitting parameter
W_b	scour base width
W_t	top scour width
y	pile displacement
z	depth below original mudline
z_{add}	additional soil depth
$z_{add,LN}$	additional soil depth to account for local narrow scour
$z_{add,LW}$	additional soil depth to account for local wide scour
z_{equ}	equivalent scour depth
γ	unit weight of sand
δ	additional soil depth factor
θ	pile rotation
$\tilde{\theta}$	normalized pile rotation
$\tilde{\theta}_{AAR}$	normalized allowable accumulated rotation
φ_{cr}	critical friction angle of sand
ω	scour slope angle